Journal of Materials Chemistry A

PAPER

View Article Online
View Journal | View Issue

Cite this: J. Mater. Chem. A, 2014, 2, 14690

Reducibility of Co at the $La_{0.8}Sr_{0.2}CoO_3$/$(La_{0.5}Sr_{0.5})_2CoO_4$ hetero-interface at elevated temperatures†

Nikolai Tsvetkov, Yan Chen and Bilge Yildiz*

Received 16th April 2014
Accepted 30th June 2014

DOI: 10.1039/c4ta01889c

www.rsc.org/MaterialsA

The fast kinetics of oxygen reduction reaction (ORR) at oxide hetero-structures made of $La_{0.8}Sr_{0.2}CoO_3$ and $(La_{0.5}Sr_{0.5})_2CoO_4$ ($LSC_{113/214}$) attracted great interest to enable high performance cathodes for solid oxide fuel cells. The aim of this work is to uncover the underlying mechanism of fast ORR kinetics at the $LSC_{113/214}$ system from a defect chemistry and electronic structure perspective. X-ray photoelectron spectroscopy with depth profiling was used to compare the reducibility of the Co cation and the valence band offset in the $LSC_{113/214}$ multilayer (ML) and in single phase LSC_{113} and LSC_{214} films. At 250 °C, the Co 2p core-level photoelectron spectra showed the presence of Co^{2+} across the ML interfaces in both the LSC_{113} and LSC_{214} layers. While this is similar to the Co valence state of LSC_{113} single phase films, it is contrary to the single phase LSC_{214} films which had only the higher oxidation state of cobalt, Co^{3+}. The greater reducibility of Co in LSC_{214} in the ML structure compared to that of Co in the LSC_{214} single phase film was attributed to electron donation and transfer of oxygen vacancies from LSC_{113} across the interfaces, and it is one mechanism to enhance the oxygen reduction activity at the $LSC_{113/214}$ hetero-structure.

Introduction

Solid oxide fuel cells (SOFC) are electrochemical devices to convert chemical energy in fuels to electrical energy, with efficiency far exceeding that of traditional internal combustion engines. The efficient energy conversion by SOFC currently requires elevated temperatures of around 800 °C or higher.[1] Lowering of operating temperature to the intermediate range, 500–700 °C, is desirable for better lifetime and reduced costs, but it also hinders the energy conversion efficiency primarily due to the slow oxygen reduction reaction at the cathode.[2] Extensive efforts have been dedicated to the design of new cathode materials with fast oxygen reduction kinetics, by increasing availability and mobility of oxygen vacancies and concentration of conduction band electrons.[1–4]

Hybrid structures, such as nanoscale composites of two materials, for example in the form of multilayers with a high density of hereto-interfaces, have recently drawn significant attention due to the reported superior electronic and ionic transport properties compared to single phase structures.[5–9] One example to this growing field has been the 1000-fold faster oxygen exchange kinetics found at the $LSC_{113/214}$ interfaces.[6,8,9] In our recent work, using *in situ* scanning tunneling spectroscopy (STS) combined with focused ion beam milling, we uncovered an electronic activation of a wide-band-gap oxide, LSC_{214}, when it is in contact with the LSC_{113} in a multilayer (ML) geometry.[10] By electronic activation, we mean the disappearance of the apparent energy gap in LSC_{214} at and above 250 °C, contrary to the presence of about 1 eV energy gap in LSC_{214} single phase thin films at the same conditions. Electrons in the conduction band of oxides, or similarly the surface electronegativity of oxides, are important in determining the ability of the surface to donate electrons to adsorbates, governing the electrochemical reactivity of the surface.[3,11,12] Therefore, such electronic activation, combined with the fast oxygen exchange path of LSC_{214} along the rock-salt layers,[13] could provide one important mechanism for accelerating the oxygen reduction reaction kinetics on the $LSC_{113/214}$ nano-composites.

While this interesting behavior was observed from an electronic structure perspective alone in our recent work,[10] the current paper provides chemical evidence, in particular on the oxidation state of Co and the valence band structure, which also supports and correlates well with the electronic activation of LSC_{214} when in contact with LSC_{113}. Co oxidation state is proportional to the concentration of oxygen vacancies in LSC_{113} and oxygen interstitials in LSC_{114}. Therefore, the knowledge of the Co oxidation state near the $LSC_{113/214}$ interface makes it possible to deduce whether the electronic activation found in

Laboratory for Electrochemical Interfaces, Department of Nuclear Science and Engineering, Massachusetts Institute of Technology, 77 Massachusetts Avenue, Cambridge, Massachusetts 02139, USA. E-mail: byildiz@mit.edu

† Electronic supplementary information (ESI) available: O 1s, Sr 3d, La 3d and Co 2p XPS core-level spectra obtained from the LSC_{113} and LSC_{214} layers in the ML structure and in single phase films at room temperature, and the elemental analysis obtained from XPS depth profiling in single phase LSC_{113}, LSC_{214} and ML at room temperature and at 250 °C. See DOI: 10.1039/c4ta01889c

our previous work is accompanied by an exchange of oxygen defects. Furthermore, it also reflects the surface electronegativity.[12]

In this work, we implemented depth profiling in X-ray photoelectron spectroscopy (XPS) measurements to compare the reducibility of Co cation and the valence band edge positions in $LSC_{113/214}$ ML with that in LSC_{113} and LSC_{214} single phase films at room temperature and at 250 °C. The results will describe the reducibility of Co in the different sample configurations measured by XPS. We found that, when LSC_{214} is in the multilayer configuration, Co is less reduced in comparison to that in the single phase film at room temperature. On the other hand, when the temperature is raised up to 250 °C, the opposite situation takes place: Co is reduced to a greater extent in the LSC_{214} in ML than that in LSC_{214} single phase film. The observed results will be discussed based on the measured differences of the electronic band structure of $LSC_{113/214}$ junction at different temperatures and the corresponding exchange of electronic and ionic defects at the interface.

Experimental

$La_{0.8}Sr_{0.2}CoO_3$ and $(La_{0.5}Sr_{0.5})_2CoO_4$ films in the ML and single phase configurations were deposited onto $SrTiO_3$ single-crystal substrates using pulsed laser deposition method with a KrF excimer laser of 248 nm wavelength. The films were deposited at 700 °C under 10 mTorr oxygen pressure. After the growth process, the films were cooled down to room temperature in 2 Torr oxygen pressure to oxidize them. The thickness of the single phase and the ML films was around 70 nm and 130 nm, respectively.

Depth-resolved X-ray photoelectron spectroscopy measurements for all the samples (LSC_{113}, LSC_{214} and $LSC_{113/214}$) were performed using the Perkin-Elmer PHI-5500 ESCA Spectrometer with monochromated Al Kα (1486.65 eV) X-ray radiation equipped with charge neutralization system under a base pressure of 10^{-9} Torr. The XPS depth profiling was used to assess the chemical composition of the buried layers within $LSC_{113/214}$ ML interface. Sputter etching was carried out by the EX05 Ar^+ ion gun, with 1 kV ion beam energy and 0.5 mA beam current on the area of 2 × 2 mm^2. X-ray photoelectron spectra upon sputtering in each layer were obtained at an emission angle of 45°. In some cases angle-resolved XPS measurements were performed by changing of emission angle from 0° to 70° relative to surface normal. The probing depth at 0° was 6 nm, 4 nm and 4 nm for Sr 3d, La 3d, and Co 2p, respectively. Tilting the sample to 45° and 70° leads to a decrease of the probing depth down to 71% and 34%, respectively, of that at 0°.

The energy at valence band maximum was determined by a linear extrapolation of the steep leading edge of the highest valence-band peak to the baseline.[14,15] The core-level binding energy positions were defined as the center of the peak width at the half of the peak height. The binding energies were calibrated with a reference to C 1s peak at 284.80 eV. For relative representation in Fig. 1c, the (La + Sr)/Co ratio was normalized to be equal to 1 within the middle of the LSC_{113} layers.

TEM measurements were performed using JEOL 2010 FEG microscope. TEM samples were fabricated in the Helios

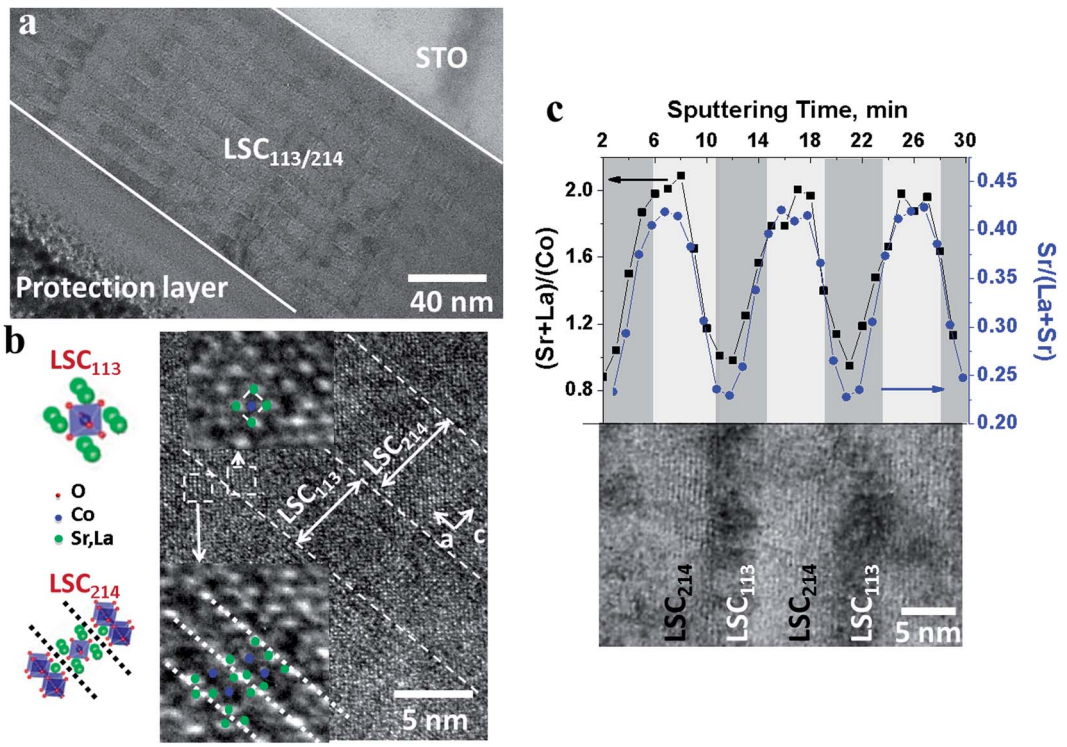

Fig. 1 (a) Transmission electron microscope (TEM) image and (b) high resolution TEM image of the $LSC_{214/113}$ multilayer cross-section. (c) Compositional depth profile obtained by XPS, overlapped onto the TEM image of corresponding layers at the $LSC_{214/113}$ multilayer system.

Nanolab 600 dual beam focused ion beam milling system using Ga ion beam operated at a voltage and current that was varied in range of 30 keV–5 keV and 9.5 nA–28 pA, respectively.

Results and discussion

Structure and composition of the $LSC_{113/214}$ thin film multilayer

X-ray diffraction analysis on the $LSC_{113/214}$ thin film multilayer structure used in this work was described in our previous report and revealed the presence of (001)-oriented LSC_{113} and LSC_{214} phases.[10] Fig. 1a and b show the cross-sectional transmission electron microscopy (TEM) images of the $LSC_{113/214}$. The thickness of LSC_{113} layers is around 5–6 nm and the thickness of LSC_{214} layers is around 7–8 nm. Alternating regions assigned to LSC_{113} cubic perovskite and LSC_{214} Ruddlesden-Popper phases can be distinguished at the atomic level (Fig. 1b), although the TEM image indicates the presence of defected regions, formed probably during the ion milling process.

Fig. 1c shows XPS depth profile across the multilayer. The regions with high and low Co/Sr ratio are LSC_{113} and LSC_{214} phases, respectively. Sr-fraction was not found to exhibit any detectable increase at the LSC_{214}–LSC_{113} interfaces, unlike recent theoretical predictions.[16] By combining the TEM measurements and compositional analysis from XPS, the sputtering rate was estimated to be of around 1.4 nm min^{-1} at room temperature. The gradual, rather than sharp transitions of compositions across the interfaces in Fig. 1c arise from the finite penetration depth of Sr 3d, La 3d and Co 2p photoelectrons, with a mean sampling depth (at the emission angle of 45°) of 4 nm, 3 nm and 3 nm, respectively.

Co reduction state and valence band structure at room temperature

At room temperature, in both the ML and the single phase films, Co near the surface region was found to reduce significantly during the first few minutes of Ar^+ sputtering. Fig. 2a shows the atomic ratio of the oxygen to metals, O/(La + Sr + Co), for the single phase LSC films. The steady-state level of reduction which is quite similar for both the LSC_{113} and the LSC_{214} was achieved after about 5 minutes of sputtering. This is not unexpected, because the oxygen deficiency induced by sputtering is related with the higher sputtering yield for oxygen atoms in comparison to that of metals.[17] Sputtering induced reduction of the oxygen content was similarly reported also on other metal oxides, including nickelates and cobaltites.[17,18] No other change was found for the binding energy or width of La and Sr core-level peaks, indicating that oxidation state of these cations – Sr^{2+} and La^{3+} – remains stable as the sputtering progressed into the material (Fig. S1,† ESI). While the sputtering induced reduction could be seen as an artefact, the differences in the Co reduction state upon sputtering could also allow us to compare the "ease" of reduction in LSC_{214} and LSC_{113} when treated at the same environment in terms of sputtering conditions and temperature. At steady state the oxygen content no longer depends on the sputtering fluency but depends only on the enthalpy of oxygen vacancy formation[17] – a measure of the reducibility. Along with the decrease of oxygen content shown in Fig. 2a, the formation of an additional peak in Co 2p core-level spectra can be observed in Fig. 2b. The initial Co $2p_{3/2}$ peak centered at 780.7 eV was attributed to Co^{3+}.[19] The additional peaks centered at 779.0 eV were attributed to the Co^0.[18] Thus, sputtering at room temperature in vacuum was found to lead to the reduction of the oxide surface.

Co^0 peak intensity increased as the emission angle decreased (more surface sensitive geometry) during the XPS measurements (Fig. 2c). The presence of Co^0 in the spectra was attributed to the localization of electrons on the Co site when oxygen is removed from the lattice on/near the surface, and it does not necessarily mean the formation of metallic clusters of Co at the surface.[18] If metallic Co clusters were forming at the surface, one can expect a significant increase of Co/(Sr + La) ratio, however, we did not observe such an increase of Co content at the surface.

For comparison of the Co reduction state in LSC_{113} and LSC_{214} in single phase and multilayer configurations at room temperature, on the Fig. 3a and b the typical Co 2p core-level emission spectra obtained from the sputtered samples are

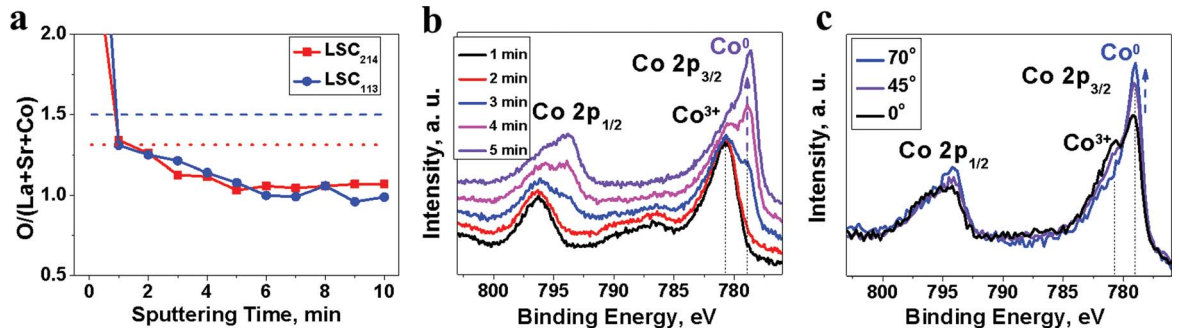

Fig. 2 (a) Evolution of oxygen content, O/(La + Sr + Co) in LSC_{214} and LSC_{113} in single phase films during sputtering. Dashed and dotted lines indicates the stoichiometric O/(La + Sr + Co) ratio for LSC_{113} and LSC_{214} bulk, respectively. (b) Corresponding change of Co 2p photoelectron peak in single phase LSC_{113} as a function of sputtering time at room temperature. (c) Co 2p photoelectron spectra obtained from reduced LSC_{214} layers in $LSC_{113/214}$ at different emission angles. The photoemission depth from the surface for Co 2p photoelectrons was calculated to be around 3 nm, 2 nm, and 1 nm at the emission angles (relative to surface normal) of 0°, 45°, and 70°, respectively.

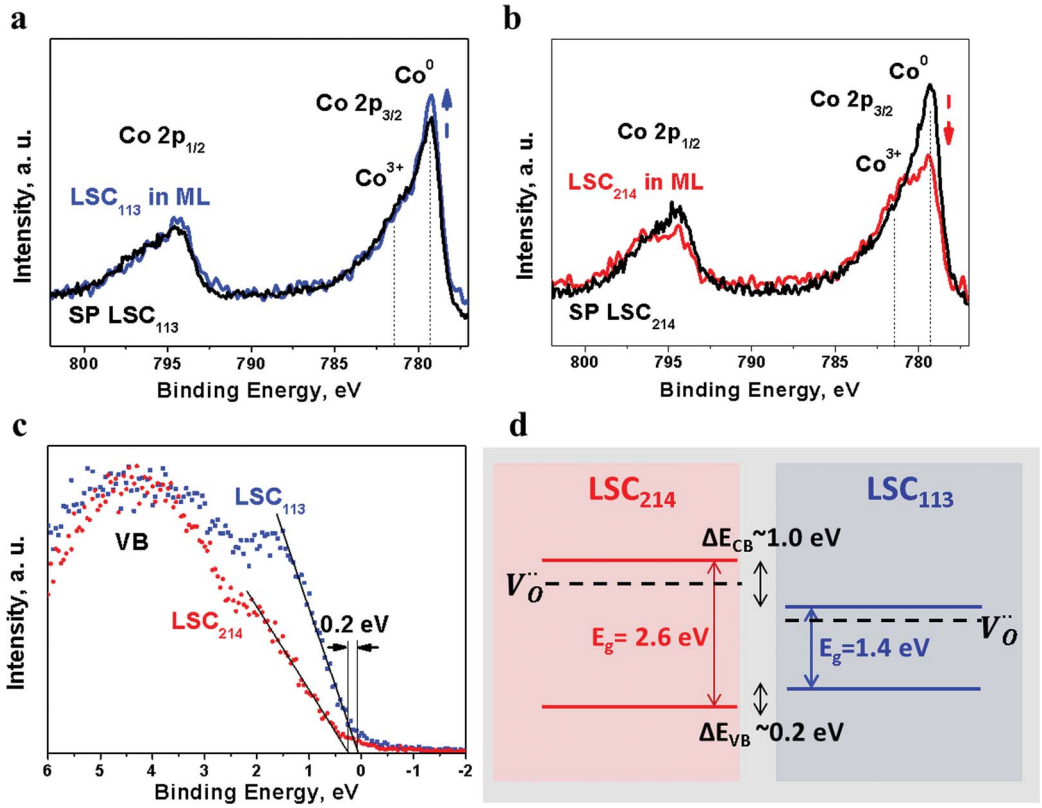

Fig. 3 Typical Co 2p core-level photoelectron spectra from sputtered (a) LSC_{113} and (b) LSC_{214} films in single phase (SP) and multilayer (ML) configurations recorded at room temperature. (c) Valence band (VB) spectra of LSC_{113} and LSC_{214} films recorded at room temperature. (d) Energy band diagram of $LSC_{113/214}$ junction at room temperature constructed by using the valence band offset of 0.2 eV determined using XPS in this work (c) and band gap values of 2.6 eV and 1.4 eV obtained by tunneling spectroscopy in ref. 10. Dashed lines schematically show the relative position of the shallow donor levels arising from the oxygen vacancy defects in reduced LSC_{113} and LSC_{214}.[20]

shown. Two peaks attributed to Co^{3+} and Co^0 can be distinguished in the spectra. A significant difference can be observed for the Co $2p_{3/2}$ spectra of LSC_{214} in going from the single phase to the multilayer configuration (Fig. 3b). The Co^0 peak intensity in LSC_{214} that is in contact with LSC_{113} was found to be less than that in single phase LSC_{214} film. The features shown in Fig. 3a–c (and also in Fig. 4a–c) are consistently observed among all the LSC_{113} and LSC_{214} layers within the ML, while the data shown here on LSC_{113} and LSC_{214} within the ML come from a specific set of buried layers, at sputtering cycles 18 and 26, respectively. The Co 2p photoelectron spectra from the LSC_{113} or LSC_{214} layers at different depths (exposed upon sputtering) within the ML stack are shown in Fig. S2† (ESI).

Therefore, we deduce that Co in LSC_{214} that is in contact with LSC_{113} is less reduced compared to the Co in single phase LSC_{214}. In the case of LSC_{113}, on the other hand, Co 2p spectra are quite similar in both the single phase and multilayer configurations, with only a slightly higher intensity of the Co^0 peak in the multilayer.

The valence band offset (VBO) of around 0.2 ± 0.1 eV at $LSC_{113/214}$ junction was determined by measuring the valence band photoelectron spectra and using a linear extrapolation of the edge to zero intensity,[15] as displayed in Fig. 3c. The observed deviation from a straight line in the low binding energy region is the valence band spectral distortion related with the occupied surface states.[21] The same VBO of around 0.2 eV, as for SP films (Fig. 3c), was also found between the LSC_{113} and LSC_{214} films in the $LSC_{113/214}$ ML (Fig. S3,† ESI).

Our previous scanning tunneling spectroscopy (STS) measurements at room temperature identified the energy gap (E_g) values for LSC_{113} and LSC_{214} as 1.4 eV and 2.6 eV, respectively.[10] By using the VBO from XPS and energy gap values from STS, the energy band diagram of LSC_{113}/LSC_{214} junction was constructed and the conduction band offset, ΔE_{CB}, was estimated to be about 1.0 eV (Fig. 3d).

As indicated in Fig. 2a, the sputtering with Ar^+ leads to the formation of the oxygen vacancies at/near the surface of our LSC_{113} and LSC_{214} specimens. Thus, when the surface of LSC_{214} is reduced upon sputtering, the electrons from LSC_{214} vacancy defect level can be transferred to the conduction band of LSC_{113} (Fig. 3d). This process could lead to an apparently less reduction of Co in the LSC_{214} in multilayer compared with the single phase LSC_{214}, as shown in Fig. 3a. At the same time, when the LSC_{113} layer is reduced by Ar^+ bombardment, the shallow donor level of LSC_{113} lies below conduction band of LSC_{214}, and thus, the electron transfer from the reduced surface of LSC_{113} to LSC_{214} is not possible at room temperature.

Here we note briefly why the donor levels arising from the oxygen vacancy defects in reduced LSC_{113} and LSC_{214} are taken to be shallow (as illustrated in Fig. 3d). Generally it is accepted

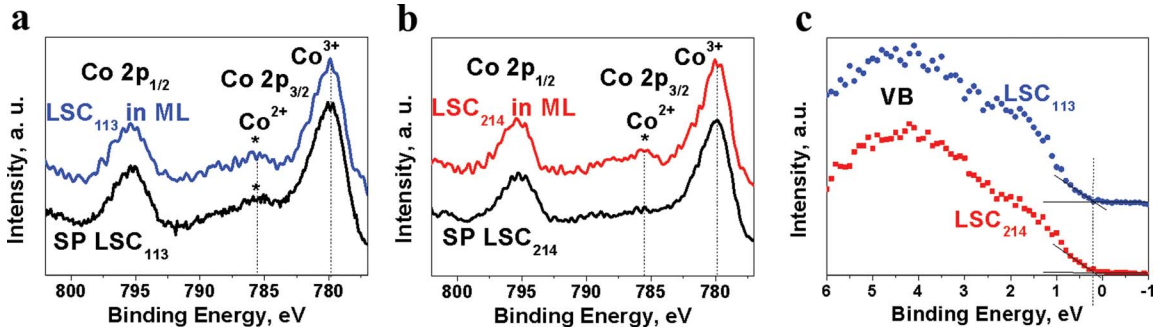

Fig. 4 Typical Co 2p core-level photoelectron spectra from sputtered (a) LSC_{113} and (b) LSC_{214} films in single phase (SP) and multilayer (ML) configurations measured at 250 °C. (c) Valence band (VB) spectra from LSC_{113} and LSC_{214} layers within the ML structure measured at 250 °C.

that for transition metal oxides the formation of the oxygen vacancies leads to the appearance of shallow donor levels.[12] Literature specifically on oxygen vacancy induced defect levels in cobaltites is scarce. However, doping oxides such as ZnO or In_2O_3 with Co leads to the formation of shallow donor level related to the introduction of oxygen vacancies.[22,23] Furthermore, the dominant oxygen vacancies in cobaltites are doubly charged oxygen vacancies[24] – defects which leads to formation of shallow donor levels.[20]

Lastly, we add that another potential mechanism for the observed difference in the reducibility of LSC_{113} and LSC_{214} in the ML configuration is the exchange of oxygen defects. Even though this process is kinetically hindered at room temperature, local heating induced by sputtering (considering that the penetration depth of Ar ions is a few nm (ref. 25)) can enable oxygen vacancy transfer from the exposed LSC_{214} into LSC_{113}. However, the oxygen vacancy transfer process from LSC_{113} to LSC_{214} is not likely because of the higher energy of formation of this kind of defect in LSC_{214} compared to that in LSC_{113}.[13]

Co reduction state and valence band structure at 250 °C

At elevated temperatures, we observe two interesting features from the Co 2p photoelectron spectra: (1) Co reduction down to the metallic state is suppressed, and (2) Co in LSC_{214} is more reduced (in the form of Co^{2+}) when in contact with LSC_{113} in the ML configuration compared to that in the single phase LSC_{214} film. Fig. 4 shows the Co 2p core-level photoelectron spectra from LSC_{113} and LSC_{214} in single phase and ML configurations at 250 °C in UHV. During the sputtering process the decrease in O content was insignificant (especially in LSC_{214}) (Fig. S4,† ESI), and the shape of Co 2p spectra shown in Fig. 4 is similar to that recorded for non-sputtered LSC compounds.[26] The presence of Co^0 was not detected in any of the samples at 250 °C. Significantly less reduction of LSC during sputtering at elevated temperatures is attributed to the oxygen mobility in these materials at elevated temperatures. The supply of oxygen from the sub-surface to the surface compensates the preferential oxygen removal during sputtering. Suppression of the sputtering-induced reduction of the transition metal cations at similar temperatures were also reported for CoO and NiO, even though these compounds have much smaller oxygen diffusion coefficients compared to LSC.[17]

In connection to the electronic activation of LSC_{214} in the $LSC_{113/214}$ ML structure previously observed by tunneling spectroscopy,[10] here we find that Co in LSC_{214} is more reduced when in contact with LSC_{113} compared to the single phase LSC_{214} film at elevated temperatures. Fig. 4a and b show Co 2p core-level photoelectron spectra from LSC_{113} and LSC_{214} films in single phase and ML configurations measured at 250 °C. The shape of the Co 2p spectra is similar for LSC_{113} both within ML and in single phase thin film (Fig. 4a), with a satellite peak by around 5–6 eV above the Co $2p_{3/2}$ peak.

The presence of such satellite peak points out the presence of the reduced state of Co, Co^{2+}.[27] On the other hand, while Co reduction down to Co^{2+} is not evident in the LSC_{214} single phase film, it is found in the LSC_{214} layers of the multilayer system (Fig. 4b). The presence of the Co^{2+} signature in LSC_{214} in the multilayer (and no such peak found in LSC_{214} single phase film) indicates that Co is more reducible in LSC_{214} when it is put in contact with LSC_{113} at elevated temperatures.

The greater reduction of Co in LSC_{214} in ML is consistent with the electronic activation found in LSC_{214} using STS across the interfaces of $LSC_{113/214}$,[10] and can be explained based on electronic and ionic defect transfer across $LSC_{113/214}$ interface. At 250 °C, the VBO was not detectable at the $LSC_{113/214}$ interface within the ML structure (Fig. 4c). The same VB maximum position was also observed across the LSC_{113} and LSC_{214} layers in the ML structure during depth profiling at 250 °C (Fig. S5,† ESI). As noted earlier, our recent STS measurements have shown that the surfaces of both of these compounds in the ML configuration have no apparent energy gap at 250 °C.[10] The absence of a VBO between the LSC_{113} and LSC_{214} layers and the absence of an energy gap in these layers in the ML structure indicates that there is no barrier for electron transfer across their interface. Therefore, the presence of Co^{2+} in LSC_{214} could indeed arise due to donation of electrons from the LSC_{113}. At the same time reduction of Co cation down to Co^{2+} can also arise because of the formation of oxygen vacancies in LSC_{214}. It is possible that oxygen vacancies are transferred from LSC_{113} into LSC_{214}, accompanied by the transfer of oxygen from LSC_{214} into LSC_{113} at the onset of the reduction in LSC_{113}. However, we cannot say unequivocally whether the oxygen from LSC_{214} is in

the form of lattice oxygen (so, an exchange of oxygen vacancies) or interstitial oxygen defects. Both electronic and ionic defect exchange mechanisms are likely in action simultaneously to maintain charge neutrality across the entirety of the LSC_{113} and LSC_{214} layers. Consequently, both the availability of excess electrons and the availability of oxygen vacancies at the surface of LSC_{214} can help assist the oxygen reduction kinetics near the $LSC_{113/214}$ interface.

Conclusions

To conclude, X-ray photoelectron spectroscopy was used to obtain insights into the chemical reasons behind the high reactivity of the $LSC_{113/214}$ interface toward oxygen reduction reaction. The results obtained here from Co 2p core level and valence band spectra combined with our recent findings from tunneling spectroscopy[10] indicate that the $LSC_{113/214}$ interface is enabling the transfer of electrons and oxygen vacancies from LSC_{113} into LSC_{214} at elevated temperatures upon the onset of the reduction of LSC_{113}. This is evidenced by the presence of Co^{2+} across both the LSC_{113} and the LSC_{214} in the multilayer hetero-structure at 250 °C, contrary to Co^{3+} being the only oxidation state in the single phase LSC_{214} film. The easier reduction of Co in the LSC_{214} when in contact with LSC_{113} in the ML configuration was attributed to the transfer of electrons and oxygen vacancies from LSC_{113} upon the reduction of LSC_{113} at elevated temperatures. Interestingly, we also found a suppression of the sputtering-induced reduction in this system at elevated temperatures. The results presented here point out the importance of the defect and electronic interactions at oxide hetero-interfaces at elevated temperatures, and their role in affecting electrochemical reactions.

Acknowledgements

We gratefully acknowledge support from the CAREER Award ("Stretching" Oxides to Low Temperature Transport and Reactivity) of the National Science Foundation, Division of Materials Research, Ceramics Program, Grant no. 1055583, and from the U.S. Department of Energy Basic Energy Sciences Division of Materials Sciences and Engineering, Grant no. DE-SC0002633. This work made use of the MRSEC Shared Experimental Facilities at MIT, supported by the National Science Foundation under award number DMR-08-19762. We thank Mr Ling Li for help with TEM sample preparation.

Notes and references

1 A. J. Jacobson, *Chem. Mater.*, 2009, **22**, 660–674.
2 H. Yokokawa and T. Horita, in *High Temperature and Solid Oxide Fuel Cells*, ed. C. S. Subhash and K. Kevin, Elsevier Science, Amsterdam, 2003, pp. 119–147.
3 W. Jung and H. L. Tuller, *Adv. Energy Mater.*, 2011, **1**, 1184–1191.
4 M. M. Kuklja, E. A. Kotomin, R. Merkle, Y. A. Mastrikov and J. Maier, *Phys. Chem. Chem. Phys.*, 2013, **15**, 5443–5471.
5 J. Garcia-Barriocanal, A. Rivera-Calzada, M. Varela, Z. Sefrioui, E. Iborra, C. Leon, S. J. Pennycook and J. Santamaria, *Science*, 2008, **321**, 676–680.
6 M. Sase, F. Hermes, K. Yashiro, K. Sato, J. Mizusaki, T. Kawada, N. Sakai and H. Yokokawa, *J. Electrochem. Soc.*, 2008, **155**, B793–B797.
7 K. Yashiro, T. Nakamura, M. Sase, F. Hermes, K. Sato, T. Kawada and J. Mizusaki, *Electrochem. Solid-State Lett.*, 2009, **12**, B135–B137.
8 E. J. Crumlin, E. Mutoro, S.-J. Ahn, G. J. la O', D. N. Leonard, A. Borisevich, M. D. Biegalski, H. M. Christen and Y. Shao-Horn, *J. Phys. Chem. Lett.*, 2010, **1**, 3149–3155.
9 M. Sase, K. Yashiro, K. Sato, J. Mizusaki, T. Kawada, N. Sakai, K. Yamaji, T. Horita and H. Yokokawa, *Solid State Ionics*, 2008, **178**, 1843–1852.
10 Y. Chen, Z. Cai, Y. Kuru, W. Ma, H. L. Tuller and B. Yildiz, *Adv. Energy Mater.*, 2013, **3**, 1221–1229.
11 N. A. Deskins, R. Rousseau and M. Dupuis, *J. Phys. Chem. C*, 2010, **114**, 5891–5897.
12 M. T. Greiner, L. Chai, M. G. Helander, W.-M. Tang and Z.-H. Lu, *Adv. Funct. Mater.*, 2012, **22**, 4557–4568.
13 J. W. Han and B. Yildiz, *Energy Environ. Sci.*, 2012, **5**, 8598–8607.
14 I. Goldfarb, D. A. A. Ohlberg, J. P. Strachan, M. D. Pickett, J. J. Yang, G. Medeiros-Ribeiro and R. S. Williams, *J. Phys. D: Appl. Phys.*, 2013, **46**, 295303.
15 A. D. Katnani and G. Margaritondo, *Phys. Rev. B: Condens. Matter Mater. Phys.*, 1983, **28**, 1944–1956.
16 M. J. Gadre, Y.-L. Lee and D. Morgan, *Phys. Chem. Chem. Phys.*, 2012, **14**, 2606–2616.
17 M. A. Langell, *Surf. Sci.*, 1987, **186**, 323–338.
18 M. A. White, T. C. Lovejoy, S. T. Ochsenbein, M. A. Olmstead and D. R. Gamelin, *J. Appl. Phys.*, 2010, **107**, 103917.
19 M. Oku and K. Hirokawa, *J. Electron Spectrosc. Relat. Phenom.*, 1976, **8**, 475–481.
20 R. S. Lubna, A. Bakhtyar, Z. Hao, W. G. Wang, Y. Q. Song, H. W. Zhang, S. I. Shah and J. Q. Xiao, *J. Phys.: Condens. Matter*, 2009, **21**, 486004.
21 E. A. Kraut, R. W. Grant, J. R. Waldrop and S. P. Kowalczyk, *Phys. Rev. B: Condens. Matter Mater. Phys.*, 1983, **28**, 1965–1977.
22 S. Dabaghmanesh, R. Saniz, M. N. Amini, D. Lamoen and B. Partoens, *J. Phys.: Condens. Matter*, 2013, **25**, 415503.
23 B. Raschid, Z. Paul, E. Emre, W. Stefan and G. Torsten, *J. Phys.: Condens. Matter*, 2014, **26**, 115801.
24 C. Simone, L. Ole Martin, F. Harald and N. Truls, *J. Phys.: Condens. Matter*, 2012, **24**, 475505.
25 T. R. Jarboe, C. W. Barnes, I. Henins, H. W. Hoida, S. O. Knox, R. K. Linford and A. R. Sherwood, *Phys. Fluids (1958–1988)*, 1984, **27**, 13–15.
26 Z. Cai, Y. Kuru, J. W. Han, Y. Chen and B. Yildiz, *J. Am. Chem. Soc.*, 2011, **133**, 17696–17704.
27 C. A. F. Vaz, D. Prabhakaran, E. I. Altman and V. E. Henrich, *Phys. Rev. B: Condens. Matter Mater. Phys.*, 2009, **80**, 155457.